Evaluation of the Biofidelity of Multibody Paediatric Human Models under Component-level, Blunt Impact and Belt Loading Conditions

K. Rawska, T. Kim, V. Bollapragada, B. Nie, J. Crandall, T. Daniel

Abstract Although multibody paediatric pedestrian human models are widely used to study pedestrian crashes, the biofidelity of these models has only been evaluated for limited loading conditions. The current study aims to evaluate the biofidelity of multibody paediatric models developed by scaling a baseline 50th percentile adult male model. The biofidelity of the baseline adult model was thoroughly evaluated prior to developing the scaled paediatric models. Next, three-year old, six-year old, and 12-year-old pedestrian human models were developed using a structure-based scaling method. Paediatric experimental data, including component-level tests on head and neck and blunt impact tests for thorax, abdomen and pelvis, were collected from the literature and used as reference responses. Simulations were performed using the paediatric models and the model responses were compared to the reference responses using an objective rating method. While the baseline adult model showed a "good" quality score in various loading conditions, the quality score of the scaled paediatric pedestrian models was rated as "acceptable". The twelve-year old model showed the best biofidelity of the three child models. This paper demonstrates the quality of the multibody paediatric human models that can be developed using only a scaling technique.

Keywords scaling, paediatric, pedestrian, head, neck, thorax, abdomen.

I. INTRODUCTION

The leading cause of death for children between the ages of 2 years and 14 years is motor vehicle crashes [1]. Although the number of child fatalities recently exhibits a decreasing trend, pedestrian fatalities still account for 20% of the fatalities of children in automotive crashes. The high fatality rate of children due to pedestrian crashes highlights the benefit of improving paediatric pedestrian protection. Improved biofidelity of paediatric human models is an important step towards improving pedestrian protection for children.

A scaling process is crucial in developing a multibody paediatric pedestrian model because of the limited biomechanical test data from child post-mortem human surrogates (PMHS) and volunteers [10]. Since the quality of the scaled model largely depends on the accuracy of the scaling technique, many authors have attempted to develop more accurate scaling techniques than employed in conventional mass-scaling technique [23-24] by considering the anatomical structure and loading conditions of the body regions of interest [2, 13, 15]. Nie et al. (2014) proposed and summarized a structure-based scaling technique in the most comprehensive manner [6]. The authors demonstrated that structure-based scaling techniques resulted in a biofidelity that was either slightly better or at least similar when compared to the mass-scaling technique for a scaled model.

Although there is less paediatric biomechanical response data in the literature than there is for adults, the paediatric data that do exist have not been fully utilized to evaluate biofidelity of paediatric models. Parent et al. 2008 [15] scaled a mid-size male adult multibody human model to paediatric models and evaluated the biofidelity of the scaled model in the thorax frontal impact condition. Forbes et al. (2008) evaluated the biofidelity of a multibody 6-year-old model by considering head-neck tension and flexion/extension, thorax frontal impact, and belt loading on abdominal regions [13]. Although the Young's modulus of children differs from that of adults for most tissues [30], the difference in the material properties was not considered and the child model demonstrated overall stiffer responses than those of the PMHS [13]. Therefore, biofidelity of the

K. Rawska is a research specialist (tel: +1 434 296 7288, fax: +1 434 296 3453, kr5df@virginia.edu), T. Kim is a research scientist, V. Bollapragada is an graduate student, B. Nie is an research associate and JR. Crandall is Professor, all at University of Virginia Center for Applied Biomechanics, Charlottesville, VA. T. Daniel is an engineer at Google, Inc.

scaled multibody paediatric model has not been evaluated by considering both geometric and material property differences between children and adults under various loading conditions and age groups [13].

This study aimed to evaluate the biofidelity of the scaled paediatric human models representing three-year old (3YO), six-year old (6YO) and 12 year old (12YO) children in various test loading conditions. The biofidelity of the baseline adult model was thoroughly evaluated prior to developing the scaled paediatric models. Then, the 3YO, 6YO and 12YO models were developed using a structure-based scaling method. Paediatric biomechanical experimental data, which included component-level tests on head and neck and blunt impact tests for thorax, abdomen and pelvis, were collected from the literature and used as reference responses. The corresponding simulations were performed using the paediatric models and the model responses were compared to the reference responses using an objective rating method.

II. METHODS

Baseline Human Model

A 50th percentile adult male model was developed by combining three independent models: the upper body was adapted from a TNO scalable facet occupant model [5] and the lower extremities were adopted from models developed by Kerrigan [3] and Hall [4] (Figure *1* (a)). The biofidelity of the combined model was improved by validation under various loading conditions. The upper body was improved by performing validation against various cadaveric blunt impact tests with the mechanical characteristics of the relevant joints and restraints updated by applying optimized scaling factors (TABLE 1). After optimization, the baseline adult pedestrian model showed good correlation with PHMS response corridors, thus serving as a basis for scaling (Figure A *1*-Figure A *5*).

TABLE 1
SUMMARY OF THE TARGET RESPONSES FOR BASELINE MODEL IN THE LITERATURE

Upper body region	Reference for the target response
Head	Head blunt impact test [19]
Neck	Neck flexion-extension test [29]
Thorax	Frontal blunt impact test [22]
Abdomen	Frontal slender bar impact test [28]
Pelvis	Lateral blunt impact test [21]

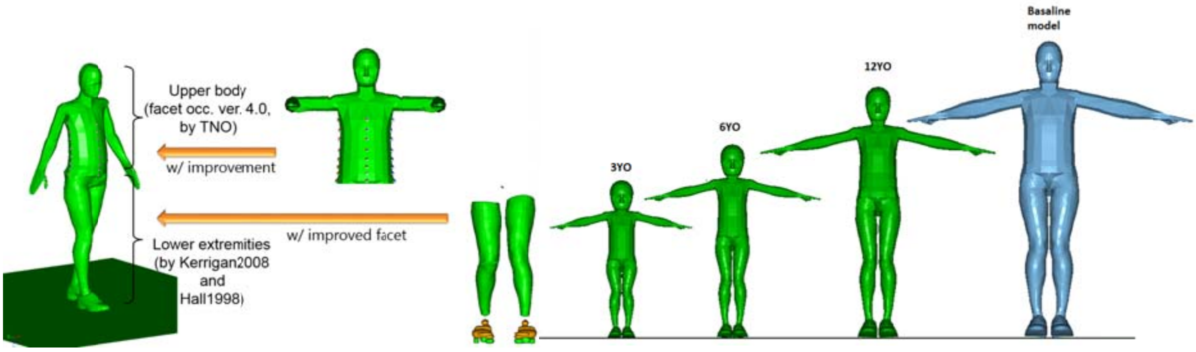

(a) Baseline model. (b) Scaled child models.

Figure 1 Baseline model and paediatric models.

Scaled Version of Paediatric Models

The structure-based scaling method proposed by Nie et al. (2014) [6] was chosen to develop 3YO, 6YO, and 12YO paediatric models (Figure *1* (b)) because this method considers anatomical structures and loading conditions as well as the anthropometry. The details of the scaling method used in the current study were described in Nie et al. (2014) [6]. The anthropometry targets for paediatric models were determined based on an anthropometry measurement study [26]. The MADYMO Generator of Body Data [27] was employed to scale the geometry and inertial properties of the baseline model and scaling factors for depth, width, and height for fourteen body regions were obtained (TABLE A *1* and TABLE A *2*). Using the scaling factors for geometry and scaling factors for Young's modulus [15], 3YO, 6YO and 12YO pedestrian models were developed by scaling the stiffness of springs defined in the joints (between bodies) and contact surfaces (TABLE A3). Since the scaling of resistance models using the structure-based scaling technique (Nie et al.) applies only to the stiffness, the damping characteristics of the models were scaled using a mass-based scaling technique [23-24].

Evaluation of the Biofidelity of Multibody Paediatric Pedestrian Human Models

Head Drop Test

The disarticulated head at the occipital joint was dropped on a rigid flat surface with 1.71 m/s and 2.43 m/s initial impact speeds for the 15 cm and 30 cm drop test conditions, respectively [19]. The forehead was positioned to face the ground in order to obtain first contact with the forehead area (Figure B 1). Contact force and head acceleration time histories were collected in the simulations. Since the reference only presented resultant acceleration time histories for a number of the subjects (Table 2), the reference acceleration time histories were generated based on the given peak and duration of the head acceleration data from the literature [19]. Since there was no direct data for 3YO, 6YO and 12YO subjects, peaks and durations of the head acceleration time histories from 9-month-old subjects to 16-year-old subjects were interpolated to obtain those for 3YO, 6YO and 12YO (*Figure 2*). Although there was large variability in the peak head acceleration for the subjects less than 1 year of age, the peak head accelerations of the subjects 1 year-old and older were similar to one another. Lastly, based on the interpolated peaks and durations of the head acceleration, head acceleration time histories were generated using a haversine function (see Results section).

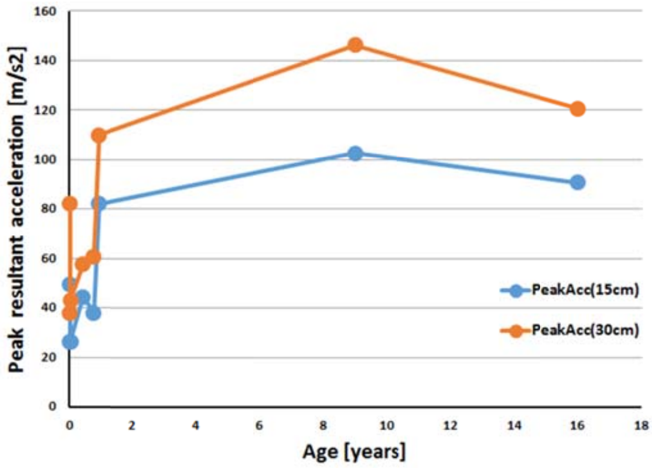

Figure 2 Head peak acceleration PMHS data with respect to subject age.

TABLE 2
HEAD DROP TEST

Age group	Drop height	Data used from PMHS tests	Model output
0–1YO: 5 subjects 9YO: 1 subject 16YO: 1 subject	15cm, 30 cm	The acceleration time history was estimated by dividing the force time history by the drop mass	Head resultant acceleration measured at the CG

Head-Neck Tensile Loading Tests

Ouyang et al. (2005) performed head-neck tensile distraction tests using paediatric PMHS aged from 2 years to 12 years old [7]. Each subject was potted at the level of T2, and then placed in a mini-Bionix MTS machine that allowed only pure axial tensile loading. To keep natural cervical lordosis, the T1-T2 was positioned at a negative 21 degrees. In the simulations, a vertically oriented translational joint was connected to a fixture rigid body, which was connected to the center of gravity (CG) of the head body through a revolute joint (Figure B *2*). The T2 body was rigidly fixed to the reference frame to mimic the potting at the level of T2 used in the experiment. Displacement time histories were imposed onto the fixture body with head rotation in the flexion/extension allowed. The tensile force measured at the potting versus the fixture displacement was compared to that of the PMHS. Since the PMHS experienced neck injury during the experiment, the responses of the model and the PMHS were compared until the average displacement at the peak values of the PMHS (TABLE 3).

TABLE 3
OUYANG HEAD-NECK COMPONENT TENSILE TEST

Age group	Elongation rate [mm/s]	Data used from PMHS tests	Model output
3YO: 3, 2 subjects 6YO: 5–7, 3 subjects 12YO: 7–12, 2 subjects	5 mm/s	Tensile force was measured by multi axial load cell at a distal end of the potted head-neck complex, thus displacement was recorded by displacement transducer in the crosshead of the MTS machine	Head neck tensile force was measured at T1 load cell level as a joint constraint definition

Thoracic Frontal Blunt Impact

Ouyang et al. (2006) conducted a series of frontal thoracic impactor tests on paediatric subjects. Detailed information about impactor mass, dimension, impact velocity and instrumentation were collected in TABLE 4 [8]. The model was positioned on a plate with head and spine erected and with the arms positioned horizontally. Thoracic impact point was set down at the fourth thoracic vertebra (Figure B *3*).

TABLE 4

OUYANG FRONTAL THORACIC IMPACT TESTS INTRODUCED TO THIS STUDY – INITIAL CONDITIONS

Age group	Impactor mass	Impactor diameter	Impactor surface	Impactor speed	Data used from PMHS tests	Model output
3YO: 2–3, 3 subjects	2.5 kg	50 mm	no padding	6.0 m/s	Chest deflection: calculated based on photo targets and chestband data.	Chest displacement: Relative distance between T4 body and Impactor body
6YO: 5–7, 3 subjects	3.5 kg	75 mm				
12YO: 7–12, 3 subjects						

Table Top Belt Pull Test on Thoracic Region

Kent et al. (2011) tested a 6-year-old PMHS to determine thorax force-deformation responses under belt loading conditions [9]. Simulations were performed with the child models placed directly on a rigid flat surface, and the belt was positioned on the chest of the model according to each test condition (TABLE 5). A pre-simulation was performed to obtain static equilibrium of the scaled child model resting on the rigid surface. Then, the thorax of the pre-simulated model was loaded by either the 50 mm wide belt or the 168 mm wide belt. To be consistent with the experiment, 8 N of initial belt tension was applied to the belt model. Lastly, belt pulling displacement time histories from the experiment were applied to the belt model as input conditions (Figure B 4). The belt tension time histories measured during the simulations were compared to belt tension output from the experiment.

TABLE 5

SUMMARY OF PAEDIATRIC PMHS THORAX BELT LOADING TESTS IN THE LITERATURE

AGE GROUP	SET-UP		BOUNDARY CONDITIONS	DATA USED FROM PMHS TESTS	MODEL OUTPUT	INPUT FUNCTIONS
6YO: 1 subject	Distributed loading	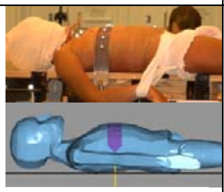	50 mm-wide belt dynamic loading	Belt force: sum of measured belt tension of both belt ends	Belt force: constraint joint force measured at joint responsible for pulling belt	Figure B 4
6YO: 1 subject	Distributed loading	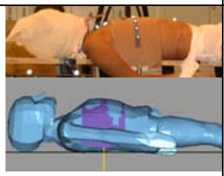	168 mm-wide belt, dynamic loading			

Table Top Belt Pull Test on Abdominal Region

The same subject used for thorax belt loading test was used in an abdominal loading study [9]. Steps similar to those used for the thorax setup were followed with respect to model positioning and application of the initial belt loading. Then, either the lower or upper abdomen was dynamically loaded by the 50 mm wide belt (TABLE 6). Additionally, a quasi-static test was performed for the lower abdomen. Belt pulling displacement time histories from the experiment served as input data (Figure B). The belt tension time histories measured during the simulations were compared to the belt tension output from the experiment.

TABLE 6
SUMMARY OF PAEDIATRIC PMHS ABDOMEN BELT LOADING TESTS IN THE LITERATURE

<table>
<tr><th>Age group</th><th colspan="2">Set-up</th><th>Boundary conditions</th><th>Data used from PMHS tests</th><th>Model output</th><th>Input functions</th></tr>
<tr><td>6YO: 1 subject</td><td>Distributed loading</td><td>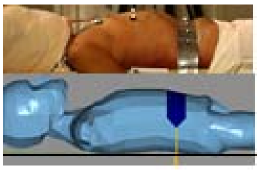</td><td>50 mm-wide belt, quasi-static, and dynamic loading</td><td rowspan="2">Belt force: sum of measured belt tension of both belt ends</td><td rowspan="2">Belt force: constraint joint force measured at joint responsible for pulling belt</td><td rowspan="2">Figure B</td></tr>
<tr><td>6YO: 1 subject</td><td>Distributed loading</td><td>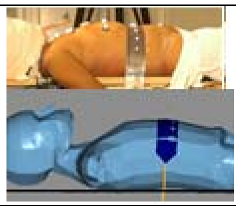</td><td>50 mm-wide belt, dynamic loading</td></tr>
</table>

Abdomen Frontal Impact Test

Ouyang et al. 2006 performed abdominal blunt impact tests using the same paediatric PMHS and the test apparatus as those used for the thoracic frontal impact tests (TABLE 7) [10]. The subject was positioned in a seated posture on a rigid plate. The arms were supported using a support fixture that allowed free horizontal motion of the arms (Figure B6). The impactor was in free flight prior to the contact with the subject. The head of the subject was supported in an upright position using a cervical collar and tape. The impact location was selected as the position one-third the distance from the umbilicus to the bottom of the sternum. The force-deflection curves of the PMHS and the models were compared for biofidelity evaluation.

TABLE 7
OUYANG FRONTAL ABDOMEN IMPACT TEST

<table>
<tr><th>Age group</th><th>Impactor mass</th><th>Impactor diameter</th><th>Impactor surface</th><th>Impactor speed</th><th>Data used from PMHS tests</th><th>Model output</th></tr>
<tr><td>3YO: 2–3, 3 subjects</td><td>2.5 kg</td><td>50 mm</td><td rowspan="3">no padding</td><td rowspan="3">6.3 m/s</td><td rowspan="3">Abdomen deflection: measured relative displacement between L3 and impactor using photo targets</td><td rowspan="3">Relative distance between L3 body and Impactor body</td></tr>
<tr><td>6YO: 5–7, 3 subjects</td><td rowspan="2">3.5 kg</td><td rowspan="2">75 mm</td></tr>
<tr><td>12YO: 7–12, 2 subjects</td></tr>
</table>

Pelvis Lateral Impact

The models were positioned such that the right side of the pelvis was facing the rectangular-shaped impactor for a lateral impact following the Ouyang et al.'s 2003 test set-up [11]. The left side of the pelvis was firmly positioned against the rear support and the buttocks were in full contact with the test table (Figure B7). The head and torso of the subjects were fixed with tape onto the support device to secure the subject's posture during the experiment. The legs were positioned perpendicular to the impact direction of impact and were allowed unconstrained motion. The test set-up was modelled using the scaled model (TABLE 8), and pelvic impact force versus pelvic deflection of the models was compared to those of the PMHS.

TABLE 8
OUYANG LATERAL PELVIS IMPACT TEST

Age group	Impactor mass	Impactor diameter	Impactor surface	Impactor speed	Data used from PMHS tests	Model output
3YO: 2–3, 3 subjects	3.24 kg	W 180 mm x H 140 mm	no padding	7.5 m/s	Pelvis deformation was obtained through photo target analysis	Pelvis deflection: relative distance between Sacrum body and Impactor body
6YO: 5–7, 3 subjects						
12YO: 7–12, 2 subjects						

Biofidelity Evaluation

Biofidelity of the paediatric models was evaluated using the MADYMO Objective Rating tool [25][31]. Three quality scores – Global Peak Value, Global Peak Time and Weighted Integrated Score – were calculated using each model's response and the corresponding PMHS response. The final score was calculated as an average of the three parameters described below.

a) Global Peak Value/Timing combines global minimum value and global maximum value. The algorithm compares the absolute minimum and maximum value of the experimental signal.
b) Weighted Integrated Score (WIS) is a root mean square over the curve data samples. The very small value was introduced to avoid a division by zero [25] [31].

WIS is defined as follows:

$$Score\ (WIS) = 1 - \sqrt{\frac{\sum(W*((1-crit)^2))}{\max(\delta,\sum W)}}, \delta\text{=1.0E-06,} \qquad (1)$$

Objective Rating calculates scores based on WIS using the Factor Method (WiFac). Effectively this means that every local score is selected such that it contributes to the total score just as the function value would contribute to total area underneath the graph. The formulation is displayed below [25][31]:

$$Score_{WiFac} = \sqrt{\frac{\sum(\max(f[n^2])*\left(1-\frac{\max(0,f[n]*g[n])}{\max(\delta,f[n]^2,g[n]^2)}\right)^2}{\max(\delta\sum\max(f,[n]^2,g[n]^2))}}, \delta\text{=1.0E-06,} \qquad (2)$$

Finally, to describe model quality, rating was divided into four equal intervals: 0–25% (P) (red); 26–50% (M) (orange); 51–75% (A) (yellow); 75–100% (G) (green).

III. RESULTS

Head Drop Test

For all age groups, resultant head accelerations showed similar trends for the 15 cm and 30 cm drop heights (Figure *3* and Figure *4*). The smallest correlation in terms of peak magnitude was observed in the 3YO model but the correlation increased with the age represented by the model. The best timing correlation with the experimental response can be observed in the 12YO model response. The resultant accelerations were higher than the PMHS response by about 12% on average.

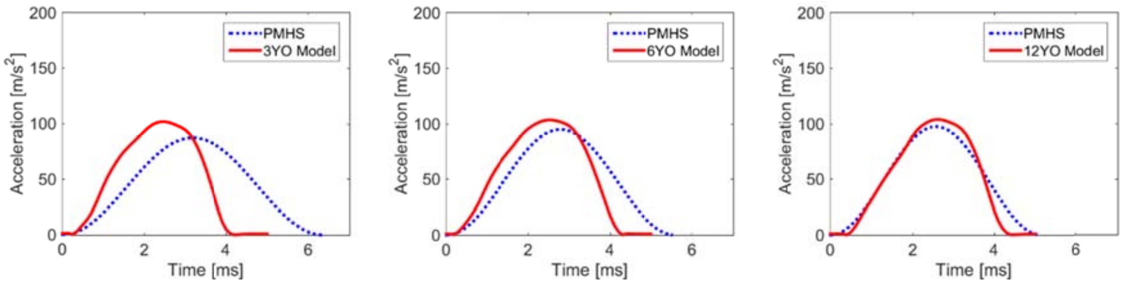

(a) 3YO. (b) 6YO. (c) 12YO.

Figure 3. Comparison between the estimated PMHS head acceleration and model head acceleration (15 cm drop).

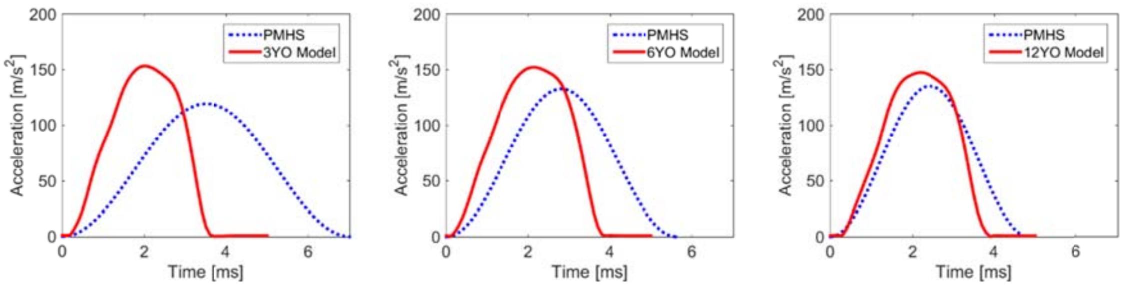

(a) 3YO. (b) 6YO. (c) 12YO.

Figure 4. Comparison between the estimated PMHS head acceleration and model head acceleration (30 cm drop).

Head-Neck Tensile Test

The head-neck tensile results were more compliant in the loading phase for all the scaled paediatric models. Only the 3YO model reached a similar force value to the individual PMHS responses (Figure *5*(a)). The other two models reached slightly lower force values than did the subjects in this test mode. Paediatric data should be considered only to an average displacement of 20.2 (+-3.2) mm and average force equal to 725.9N+-171.0 N, due to subject failure.

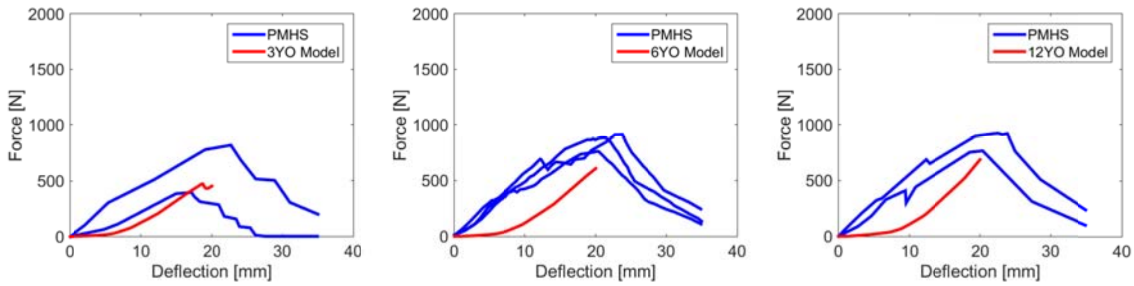

(a) 3YO. (b) 6YO. (c) 12YO.

Figure 5. Comparison between the models measured neck force-deflection and the PMHS individual response.

Thoracic Frontal Blunt Impact

The paediatric models showed more compliant responses than the PMHS during the lower chest deflection (Figure *6*). The thorax of the 3YO model stiffened upon further thorax deformation until reaching approximately 23 mm of the chest deflection. The peak impact force of the 3YO model was close to that of the PMHS, but the peak chest deflection was about 10%-30% greater than that of the PMHS (Figure *6* (a)). The 6YO model exhibited lower peak force than that of the PMHS (Figure *6* (b)), but the peak thorax deflection was close to the experimental data. The 12YO showed stiffer response than the PMHS; however, the initial thorax stiffness followed the experimental response. The 12YO showed softer response than the PMHS, and the achieved maximum chest deflection was around 15 percent greater than the available response of the 12YO subject (Figure *6* (c)).

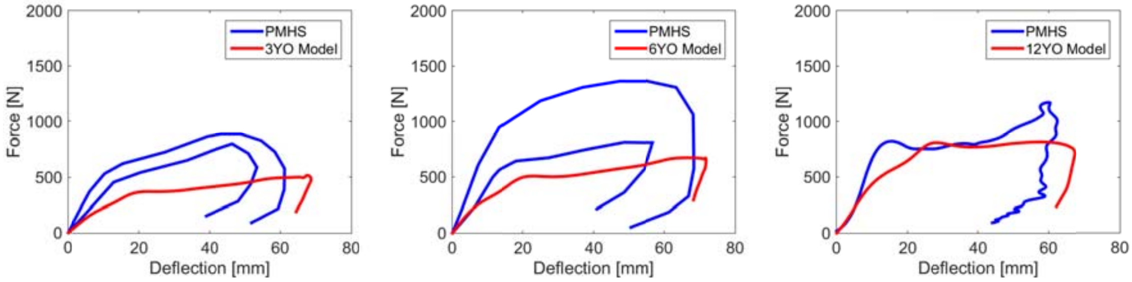

(a) 3YO. (b) 6YO. (c) 12YO.

Figure 6. Comparison between the measured model thorax force-deflection and the PMHS corridor (a), (b), and individual response (c).

Thoracic Frontal Belt Loading

Under the thoracic frontal belt loading conditions with the 50 mm-wide and the 168 mm-wide belts, the 6YO model showed slightly lower belt pull forces than those of the PMHS (Figure 7). For the distributed belt loading condition, the 6YO model showed 25% (Figure 7 (a)) to 75 % (*Figure* 7 (b)) lower peak force than the PMHS.

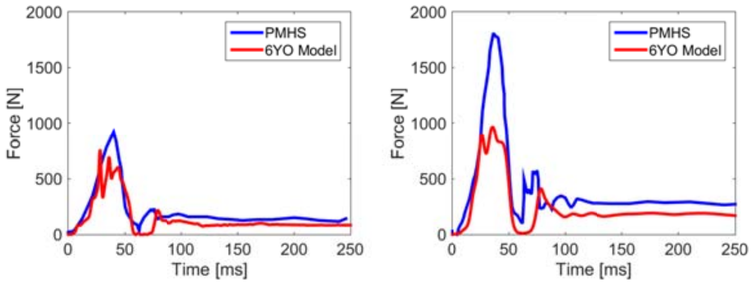

(a) 50 mm-wide belt. (b) 168 mm-wide belt.

Figure 7. Comparison of belt forces of the 6YO model and the PMHS (distributed loading).

Abdominal Frontal Blunt Impact

Under the abdominal frontal blunt impact condition, the paediatric models showed substantially stiffer responses than did the PMHS (Figure *8*). The abdomen of the 3YO model showed initially stiffer behavior, while the 6YO and 12YO models matched the PMHS initial responses. The 3YO model showed force levels similar to the experimental values. The 6YO and 12YO model exhibited the peak force almost 100% compared to that of the PMHS. While the paediatric models over-predicted the peak abdominal impact forces, these models showed around 30% to 60% less abdominal deflection than those of the PMHS.

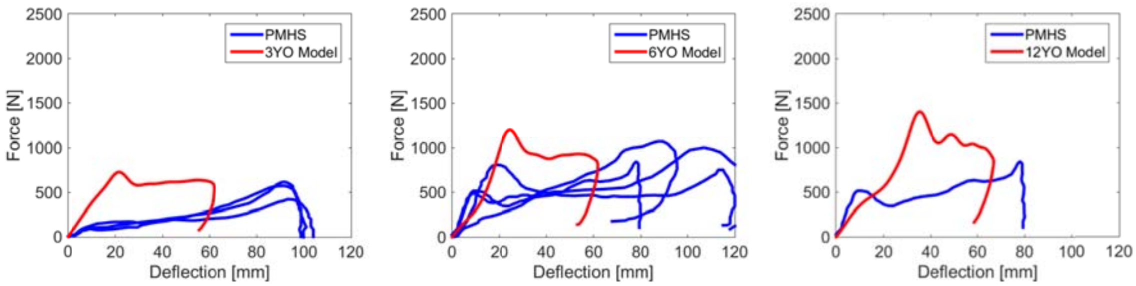

(a) 3YO. (b) 6YO. (c) 12YO.

Figure 8. Comparison between the measured abdomen force-deflection and individual PMHS response.

Abdominal Frontal Belt Loading

Under the upper and lower abdominal dynamical belt loading conditions with the 50 mm-wide belt, the 6YO model showed lower belt pull forces than those of the PMHS (Figure 7 (b) and (c)). Nevertheless, for the lower abdomen the quasi belt loading condition (Figure 7 (a)) showed good correlation with the PMHS experimental data.

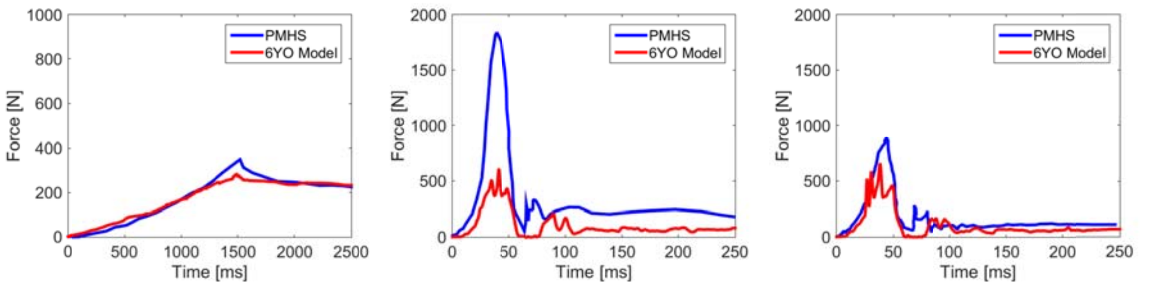

(a) lower abdomen (quasi-static) (b) lower abdomen (dynamic) (c) upper abdomen (dynamic)

Figure 9. Comparison of belt forces of the 6YO model and the PMHS (distributed loading).

Pelvic Lateral Blunt Impact

The pelvis responses of all three paediatric models were initially slightly more compliant than those of the PMHS data under low pelvic deformation (Figure *10*). The 3YO and 6YO models showed higher peak forces than those of the PMHS with later peak times. The 12YO models showed the closest peak force to those of the PMHS while only showing 66% of the peak pelvic deflection. Overall, the response for the 12YO model was the closest to the response corridor.

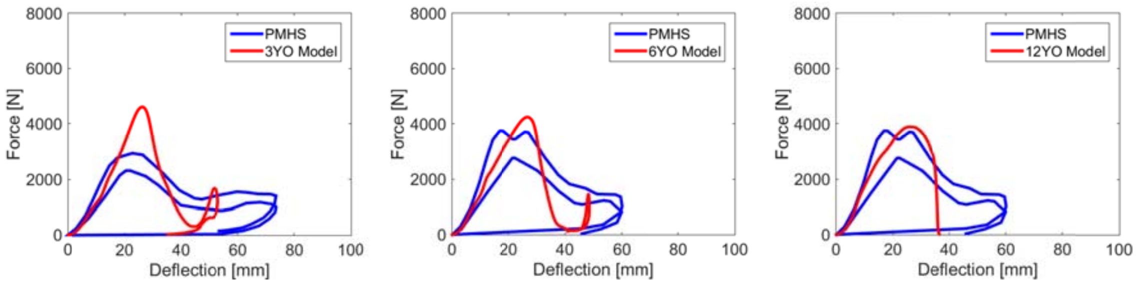

(a) 3YO. (b) 6YO. (c) 12YO.

Figure 10. Comparison between the measured model pelvis force-deflection and PMHS response.

Summary of Paediatric Model Evaluation

The experimental signals quality score for developed paediatric child dummy models are presented below (Tables 9–12). The MADYMO Objective Rating tool was employed to calculate three parameters, which serve to determine paediatric model's quality score. The exact rating method is described in the Appendix. Ratings were divided into four intervals: results with scores of 0–25% are described as (P: Poor); 26–50% as (M: Marginal); 51–75% as (A: Acceptable); and 76–100% as (G: Good).

TABLE 9
ADULT MODEL QUALITY SCORE

Body Region	Test Mode	Signal Type	Global Peak Value	Global Peak Time	WiFac	Average score
Head	15 cm drop [19]	Force-Time	94 (G)	92 (G)	71 (A)	85 (G)
	30 cm drop [19]		91 (G)	84 (G)	75 (G)	
Head-Neck	GESAC lateral [18]	AngleY-Time	87 (G)	98 (G)	83 (G)	82 (G)
		PositionY-Time	91 (G)	98 (G)	81 (G)	
		PositionZ-Time	97 (G)	3 (P)	92 (G)	
Thorax	Frontal 5.8 m/s [22]	Force-Time	79 (G)	55 (A)	74 (A)	75 (A)
	Frontal 4.3 m/s [32]	Force-Deflection	80 (G)	89 (G)	69 (G)	
	Frontal 6.7 m/s [32]	Force-Deflection	71 (A)	93 (G)	65 (A)	
Abdomen	Frontal 6.1 m/s [28]	Force-Time	83 (G)	82 (G)	76 (G)	80 (G)
Pelvis	Lateral 5.2 m/s [21]	Force-Time	79 (G)	91 (G)	57 (A)	74 (A)
	Lateral 9.8 m/s [21]	Force-Time	82 (G)	75 (G)	64 (A)	
					Final Score	79 (G)

TABLE 10
3YO MODEL QUALITY SCORE

Body Region	Test Mode	Signal Type	Global Peak Value	Global Peak Time	WiFac	Average score
Head	15 cm drop	Acceleration	93 (G)	92 (G)	76 (G)	72 (A)
	30 cm drop		79 (G)	57 (A)	32 (M)	
Head-Neck	Tension	Maximum force	62 (G)	84 (G)	58 (A)	68 (A)
Thorax	Frontal	Force-deflection	57 (A)	85 (G)	55 (A)	66 (A)
Abdomen	Frontal	Force-deflection	74 (A)	24 (A)	35 (M)	44 (M)
Pelvis	Lateral	Force-deflection	56 (A)	82 (G)	61 (A)	67 (A)
					Final Score	63 (A)

TABLE 11
6YO MODEL QUALITY SCORE

Body Region	Test Mode	Signal Type	Global Peak Value	Global Peak Time	WiFac	Average score for Body Region
Head	Loyd drop test 15 cm	Acceleration	94 (G)	89 (G)	71 (A)	79 (G)
	Loyd drop test 30 cm		89 (G)	75 (A)	55 (A)	
Head-Neck	Ouyang Tension	Maximum force	84 (G)	97 (G)	47 (M)	76 (G)
Thorax	Ouyang Frontal	Force-deflection	58 (A)	93 (G)	57 (A)	70 (A)
	Kent Distributed loading (50 mm-wide belt)	Belt tension history	74 (A)	87 (G)	56 (A)	
	Kent Distributed loading (168 mm-wide belt)	Belt tension history	54 (A)	98 (G)	55 (A)	
Abdomen	Ouyang Frontal	Force-deflection	82 (G)	28 (M)	60 (A)	64 (A)
	Kent Distributed quasi-static loading (low abdomen, 50 mm-wide belt)	Belt tension history	74 (a)	87 (G)	56 (A)	
	Kent Distributed dynamic loading (low abdomen, 50 mm-wide belt)		34 (M)	96 (G)	30 (M)	
	Kent Distributed dynamic loading (upper abdomen, 50 mm-wide belt)		74 (A)	87 (G)	56 (A)	
Pelvis	Ouyang Lateral	Force-deflection	76 (G)	72 (A)	47 (M)	65 (A)
					Final Score	71 (A)

TABLE 12
12YO MODEL QUALITY SCORE

Body Region	Test Mode	Signal Type	Global Peak Value	Global Peak Time	WiFac	Average score for Body Region
Head	Loyd drop test 15 cm	Acceleration	96 (G)	100 (G)	87 (G)	91 (G)
	Loyd drop test 30 cm		94 (G)	92 (G)	76 (G)	
Head-Neck	Ouyang Tension	Maximum force	89 (G)	93 (G)	49 (M)	77 (G)
Thorax	Ouyang Frontal	Force-deflection	97 (G)	64 (A)	84 (G)	82 (G)
Abdomen	Ouyang Frontal	Force-deflection	60 (A)	45 (M)	55 (A)	54 (A)
Pelvis	Ouyang Lateral	Force-deflection	83 (G)	75 (A)	31 (M)	63 (A)
					Final Score	73 (A)

IV.DISCUSSION

The current study is the first to evaluate biofidelity of the paediatric human models for the three age groups in combined test conditions for head, neck, thorax, abdomen, and pelvis. Based on global evaluation results, all paediatric models quality scores, except for the 3YO abdominal region, were defined as acceptable with the employed rating tool. The three scaled models demonstrated the best correlation with those of PMHS data for the head drop tests. On the other hand, the lowest quality score was achieved in the abdominal region. As expected, the 12YO model showed the closest correlation to those of the PHMS responses, while the 3YO model showed the worst correlation to the responses of the PMHS. It seems like the larger errors were introduced in the biofidelity of the scaled models as we scaled the baseline more.

The experimental responses were taken directly from reference documentation, thus, they were not scaled. Note that most of the PMHS were lighter than target models and the evaluation results of the current study may vary if the scaled responses were used in the evaluation. To minimize the influence of the subject variability, corridors or responses of the PMHS were grouped into the target ages of the paediatric models.

In this study, structure-based scaling techniques [6] were used instead of conventional mass-scaling techniques. While the mass-scaling technique performs a uniform scaling by assuming a perfect similarity between two models, structure-based scaling techniques consider direction-specific scaling factors that take into account the geometry of the model and loading condition. In this study, it was hypothesized that the structure-based scaling technique results in more biofidelic models than the mass-scaling technique, since a children is not a uniformly scaled adult (Table A1). In addition to geometric scaling, the Young's modulus ratio was also considered during the scaling. Although the Young's modulus ratios vary from body regions, the ratio based on the parietal bone were used in the current study [30, 17].

The head of the paediatric models showed 12% higher peak accelerations on average and shorter durations than those of the PMHS (Figure *3* and Figure *4*), while the baseline model showed similar peak head accelerations and pulse durations to those of the PMHS (Figure A.1). Note that the responses of the paediatric PMHS shown in Figure 3 and Figure 4 were generated using the haversine function based on the interpolated peak accelerations and pulse durations.

The necks of the paediatric models showed lower stiffness than those of the PMHS during the lower elongation range, while showing higher stiffness than those of the PMHS during the higher elongation range (Figure 5). Although the models exhibited a different shape of the force-deflection curves from those of the PMHS, the paediatric models predicted similar neck tensile forces at average deflection at failure of the PMHS. Note that the simulation was conducted until the average deflection at failure of the PMHS because the model did not consider the failure of neck.

Under the 6.0 m/s thorax frontal blunt impact condition, the paediatric models showed softer stiffness responses than those of the PMHS in the lower range of the chest deflection. It was found that the mass in the thorax region of the models was concentrated to the vertebra. Therefore, although the baseline model showed biofidelic response during frontal thoracic blunt impact simulation, it is possible that the contribution of the inertial, damping and elastic components of the baseline model during the frontal thoracic impact could be incorrect. Parent et al. (2009) showed that the scaled paediatric models response under frontal thoracic blunt impact is sensitive to the sternal mass. The softer responses of the models could be due to an inaccurate scaling law applied to the thorax region. The scaling law was derived assuming the thorax is an elastic ring with an elliptical cross-section [2], [6], but the human thorax is neither a perfect circle nor homogenous ring-like structure. The breadth and depth of the thorax of the baseline model were 319 mm and 222 mm, respectively. The rib cage consists of various components, such as ribs, sternum, and cartilage, joining the sternum, which have different structural stiffness. Therefore, it would be necessary to improve the scaling law for the thorax region to improve the biofidelity of the thorax of the scaled paediatric model. In addition, a child's thorax is more flexible than an adult's [14] and it may not have been fully captured by only using the ratios of Young's modulus and anthropometry between the child and the adult.

In addition, the 6YO model under-predicted the belt force more in the 168 mm wide belt loading condition than in the 50 mm wide belt loading condition (Figure 7). It should be noted that the current model has no coupling between upper and lower sternal regions. While the 168 mm wide belt loaded a wider thoracic region in superior and inferior directions compared to the 50 mm wide belt, the region between the upper and mid sternal region did not contribute to increase the stiffness of the thoracic region. Therefore, the thoracic region of the paediatric model evaluated in the current study will over estimate injury risk under frontal thoracic loading condition due to its soft thoracic region.

During the frontal abdominal impact, the paediatric models exhibited higher peak impact forces and lower peak deflections than those of the PMHS (*Figure 8*). It should be noted that the abdominal region of the baseline model was validated against a slender bar impact (Figure A. 4) [12]. In contrast, the 6YO model showed softer behavior than the PMHS under dynamic lateral belt loading for both upper and lower abdomen tests while the quasi-static lower abdomen belt loading test showed good correlation to the PMHS respond. The softer response under the lateral belt loading condition may partially be attributed to the contact stiffness of the back of the model. Also, there was initial clearance between the back of the model and the supporting plate due to the curvature of the spine, although there was no visible clearance on the PMHS test photos (Table 6). Furthermore, Forbes et al. (2008) indicated the same issues in the abdomen setup modeling which might have influence on the abdomen results [13].

The 6YO and 12YO models showed similar peak pelvic impact forces to those of the PMHS, but the 3YO model showed a substantially higher peak pelvic impact force than those of the PMHS (Figure 10). Note that the baseline model met response corridors (Figure A.5) for Viano et al.'s (1989) lateral pelvic impact tests (TABLE 8). Since the models under-predicted the pelvic deformation, the use of pelvic deformation from these models can under-estimate the pelvic injury risk under lateral impact.

The under-prediction of the pelvic deformation may be because the pelvises of the current pedestrian models were rigid bodies and did not deform. The pelvic deflection was obtained by allowing penetration of the impactor through the pelvic flesh surfaces with contact stiffness. Lastly, the current scaling law did not consider that the paediatric pelvis has a growth plate in the pelvic bones, which will increase the compliance of the pelvis further in addition to the lower Young's modulus than that of the adult.

Except for the pelvic lateral impact condition, the existing paediatric PMHS test data are mainly for frontal loading condition. For the lateral loading condition, there are paediatric lower extremity bending test data available [33, 20, 16]. In addition, scaled response corridors from adult PMHS test data could be used as guidelines for improving biofidelity of the paediatric models [23].

V. CONCLUSIONS

This study presents the first multifaceted assessment of 3YO, 6YO, and 12YO pedestrian models scaled from the 50th percentile adult male baseline model in various loading conditions from head to pelvis. Except for the 3YO abdominal region, all the scaled paediatric models showed "good" or "acceptable" scores based on the rating method employed in the current study. As expected, more errors were introduced the greater the age of the scaled model was from the baseline model. This implies that developmental considerations other than only Young's modulus are necessary to develop biofidelic paediatric models using scaling technique.

VI. ACKNOWLEDGEMENTS

Google, Inc. provided both technical and financial support for this study. Note that the views in expressed this paper are those of the authors and not of the sponsors.

VII. REFERENCES

[1] National Highway Traffic Safety Administration. Traffic Safety Facts 2011 DOT HS 811 767, 2013.
[2] Mertz, H. A Procedure for Normalizing Impact Response Data. *Society of Automotive Engineers (SAE)*, Paper 840884, 1984.
[3]. Hall, G. W. Biomechanical characterization and multibody modeling of the human lower extremity (doctoral dissertation), Charlottesville, VA: University of Virginia, 1998.
[4] Kerrigan, J. R. A computationally efficient mathematical model of the pedestrian lower extremity (doctoral dissertation), Charlottesville, VA: University of Virginia, 2008.
[5] TNO. MADYMO Human Body Models Manual, Madymo Facet occupant model version 4.0 Release 7.5, s.l.: TNO, 2013.
[6] Nie, B. et al. A Structure-based scaling approach for the development of paediatric multi-body human model. *Proceedings of ICRASH conference*, 2014, Malaysia.
[7] Ouyang, J. et al. Biomechanical Assessment of the Paediatric Cervical, *Spine*, 2005, Vol. 30(24):E716–E723.
[8] Ouyang, J. et al. Thoracic Impact Testing of Paediatric Cadaveric Subjects. *The Journal of TRAUMA Injury, Infection, and Critical Care*, 2006, Vol. 61:1492–1500.
[9] Kent, R. et al. Characterization of the paediatric chest and abdomen using three post mortem human subjects., *Proceedings 22nd Enhanced Safety of Vehicles (ESV) Conference*,2011,Washington, D.C., (USA).
[10] Crandall, J. R., Myers, B. S., Meaney, D. F. & Schmidtke, S. Z. Pediatric Injury Biomechanics, *Springer*, New York, 2013.

[11] Ouyang, J. et al. Experimental cadaveric study of lateral impact of the pelvis in children. *J First Mil Med Univ*, 2003, 23(5):397–408.

[12] Cavanaugh, J. M., Nyquist, G. W., Goldberg, S. J. & King, A. I. Lower Abdominal Tolerance and Response, pp:861–78, *Wayne State Univ*., USA, 1986.

[13] Forbes, P. A., van Rooij, L. Development of child human body models and simulated testing environments for the improvement of child safety. *TNO Science and Industry*, TNO report, TNO-033-HM-2007-00311, 2008.

[14] Kent, R. et al. Pediatric Thoracoabdominal Biomechanics. *Stapp Car Crash Journal*, 2009, Volume 53:373–401.

[15] Parent, D. P., Crandall, J. R., Bolton, J. R., Bass, C. R. Scaling and Optimization of Thoracic Impact Response in Pediatric Subjects. , M.S. Thesis. *University of Virginia, 2008*.

[16] Crandall, J. R. Simulating the Road Forward: the Role of Computational Modeling in Realizing Future Opportunities in Traffic Safety. *IRCOBI Conference on the Biomechanics of Impact*, 2009, York (UK).

[17] Parent, Daniel P. Scaling and optimization of thoracic impact response in paediatric subjects. Diss. University of Virginia, 2009.

[18] GESAC, Inc. Biomechanical Response Requirements of the Thor NHTSA Advanced Frontal Dummy, *Trauma Assessment Devise Development Program*, Report No: GESEC-05-03, s.l.: s.n., 2005.

[19] Loyd, A. M. et al. Impact Properties of Adult and ATD Heads. s.l. *IRCOBI Conference on the Biomechanics of Impact*, 2012, Dublin (Ireland).

[20] Miltner E, Kallieris D (1989) Quasistatische und dynamische Biegebelastung des kindlichen Oberschenkels zur Erzeugung einer Femurfraktur. Z Rechtsmed 102:535–544.

[21] Viano, D. C. et al. Biomechanics of the human chest, abdomen, and pelvis in lateral impact. *Accident Analysis & Prevention*, 1989, 21(6):553–74.

[22] Bouquet, R. et al. Thoracic and Pelvis Human Response to Impact, pp. 94-S1-O-03, *INRETS*, France, 1994.

[23] Irwin, A., Guidelines for Assessing the Biofidelity of Side Impact Dummies of Various Sizes and Ages, *Proceedings 46st Stapp Car Crash Conference*, 2002 ,Warrendale, PA.

[24] Mertz, H., Irwin, A., Melvin, J., Stanaker, R., Beebe, M. Size, Weight and Biomechanical Impact Response Requirements for Adult Size Small Female and Large Male Dummies. *Society of Automotive Engineers (SAE)*, Paper 890756, 1989.

[25] Madymo. Objective Rating version 7.5, *TASS Netherlands*, 2013.

[26] Snyder, R., Schneider, L., Owings, C., Reynolds, H., Golomb, D., Sckork, M. A., Anthropometry of Infants, Children, and Youths to Age 18 for Product Safety Design. UMHSRI-77-17, *Consumer Product Safety Commission*, Bethesda, MD, 1977.

[27]. Madymo. Utilities Manual, 2013, release 7.5, *TASS Netherlands*, 2013.

[28] Cavanaugh, J. M., Nyquist, G. W., Goldberg, S. J. & King, A. I. Lower Abdominal Tolerance and Response. SAE 861878, 1986.

[29] Wang, Y., Kim, T., Li, Y., and Crandall, J., Neck Validation of Multibody Human Model under Frontal and Lateral Impacts using an Optimization Technique, *Society of Automotive Engineers (SAE),* Paper 2015-01-1469, 2015.

[30] Irwin, A., Mertz, H., Biomechanical bases for the CRABI and Hybrid III child dummies, Proc.
Forty-First Stapp Car Crash Conference SAE, Paper Number 973317, 1997.

[31] Hovenga, P., Spit, H., Uijldert, M., and Dalenoort, A., Improved Prediction of Hybrid-III Injury Values Using Advanced Multibody Techniques and Objective Rating, *Society of Automotive Engineers (SAE*), Paper 2005-01-1307, 2005.

[32] Kroell, C. K., Schneider, D. C. & Nahum, A. M., Impact tolerance and response of the human thorax II., *Society of Automotive Engineers (SAE*), Paper Number 741187, 1974.

[33] Ouyang J, Zhu Q, Zhao W et al (2003b) Biomechanical character of extremity long bones in children.
Chin J Clin Anat 21:620–623

VIII. Appendix

Scaling of the Baseline Human Model

TABLE A 1
SCALING FACTORS FOR 14 BODY REGIONS FOR CHILD MODELS

Body region	3YO				6YO				12YO			
	λ_x	λ_y	λ_z	λ_E	λ_x	λ_y	λ_z	λ_E	λ_x	λ_y	λ_z	λ_E
Pelvis	0.59	0.50	0.55	0.475	0.65	0.56	0.65	0.667	0.82	0.74	0.59	0.99
Lumbar spine	0.65	0.49	0.55		0.71	0.54	0.65		0.90	0.71	0.65	
Abdomen	0.58	0.47	0.55		0.58	0.54	0.65		0.65	0.70	0.58	
Thoracic spine	0.70	0.50	0.55		0.78	0.57	0.65		0.99	0.71	0.70	
Rib cage	0.70	0.49	0.55		0.78	0.55	0.65		0.99	0.69	0.70	
Neck	0.68	0.68	0.55		0.73	0.73	0.65		0.84	0.84	0.68	
Head	0.91	0.85	0.78		0.95	0.89	0.83		0.98	0.93	0.91	
Clavicles	0.70	0.53	0.55		0.78	0.62	0.65		0.99	0.77	0.70	
Upper arm	0.53	0.53	0.48		0.57	0.57	0.61		0.73	0.73	0.53	
Lower arm	0.59	0.59	0.54		0.64	0.64	0.69		0.79	0.79	0.59	
Hand	0.54	0.51	0.51		0.63	0.62	0.63		0.78	0.81	0.54	
Upper leg	0.49	0.49	0.42		0.55	0.55	0.56		0.71	0.71	0.49	
Lower leg	0.56	0.56	0.54		0.62	0.62	0.69		0.81	0.81	0.56	
Feet	0.51	0.67	0.54		0.62	0.78	0.69		0.80	0.98	0.51	

TABLE A 2
ANTHROPOMETRY INFORMATION FOR CHILD MODEL (SNYDER ET AL., 1977)

Parameters	3YO			6YO			12YO		
	Reference value (cm)	Model value (cm)	Error [%]	Reference value (cm)	Model value (cm)	Error [%]	Reference value (cm)	Model value (cm)	Error [%]
Standing height	93.4	94.0	0.6%	114.6	114.5	-0.1%	148.8	147.5	-0.9%
Shoulder height	72.4	73.6	1.6%	90.6	91.6	1.1%	121.0	122.7	1.4%
Armpit height	65.2	68.4	4.9%	83.8	87.8	4.7%	112.7	116.9	3.7%
Waist height	49.3	51.0	3.4%	65.2	64.7	-0.8%	89.5	89.4	-0.1%
Seated height	54.4	54.1	-0.6%	63.4	62.5	-1.4%	76.7	75.9	-1.0%
Knee height	27.0	28.0	3.7%	34.9	34.1	-2.4%	47.5	47.3	-0.4%
Head breadth	13.4	13.3	-0.5%	13.9	13.9	-0.1%	14.6	14.2	-2.5%
Shoulder breadth	24.4	23.2	-4.8%	28.1	27.3	-2.8%	35.3	33.8	-4.2%
Waist breadth	15.9	15.5	-2.8%	18.3	17.5	-4.3%	23.4	22.6	-3.4%
Hip breadth	18.0	17.5	-3.1%	20.2	19.7	-2.6%	26.6	25.9	-2.5%
Head to Chin height	17.5	17.5	0.1%	18.4	18.6	0.8%	20.0	20.1	0.4%
Shoulder to Elbow length	16.7	16.1	-3.8%	20.7	21.3	3.1%	27.8	28.7	3.1%
Forearm-hand length	24.4	24.8	1.7%	30.2	28.8	-4.7%	40.0	38.6	-3.6%
Head length	17.5	17.1	-2.3%	18.2	17.8	-2.1%	18.8	18.5	-1.8%
Chest depth	16.6	15.8	-4.9%	18.4	18.2	-1.2%	23.3	22.2	-4.6%

TABLE A 3

SUMMARY OF THE STRUCTURAL SCALING APPROACH (NIE ET AL. 2014)

Human body part	Loading conditions	Structure mechanism	Simplified physics for varied loading on beam and ring structures	Scaling law
Long bone, spine	Axial loading	Free-end beam/ Cylinder	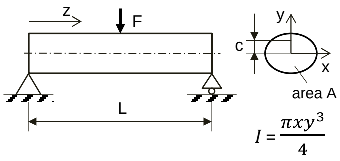	$$F = \frac{\Delta L \cdot A \cdot E}{L}$$ where L – Original length of the beam ΔL – Elongation under axial loading A – Area of the beam cross-section E – Young's modulus With scaling factors applied to the two ends, there is, $$\lambda_F = \frac{\lambda_Z\, \lambda_X\, \lambda_Y\, \lambda_E}{\lambda_Z} = \lambda_X\, \lambda_Y\, \lambda_E$$
	Shear	Free-end beam	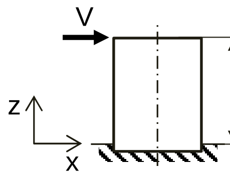	$$V \sim \tau_{max} \cdot A = \gamma G A$$ where γ – Shear strain G – Shear modulus $$\lambda_F = \lambda_G \cdot \lambda_A = \lambda_X \lambda_Y \lambda_E$$
	Lateral bending	Simply supported beam	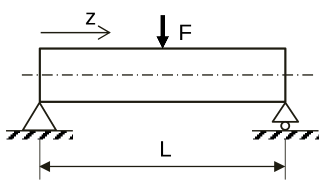	$$\sigma = \frac{M \cdot c}{I} = E\varepsilon$$ where M – Bending moment on the cross c – Distance to the neutral axis $$\lambda_M = \frac{\lambda_X\, {\lambda_Y}^3\, \lambda_E}{\lambda_Y} = \lambda_X {\lambda_Y}^2\, \lambda_E$$ λ_θ= 1
Thorax, pelvis	Lateral force	Rings (4 joints / restraints)	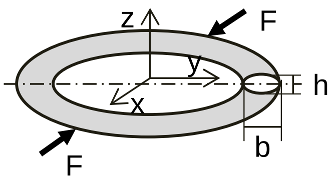	$$K = \frac{Ehb^3}{2r^3}$$ where K – Structural stiffness of a ring under lateral F h – Height of the cross section b – Width of the cross section r – Radius of the ring $$\lambda_F = \lambda_E \cdot \lambda_z \cdot \sqrt{\lambda_X\, \lambda_Y},\quad \lambda_D = \lambda_X$$

Baseline model responses

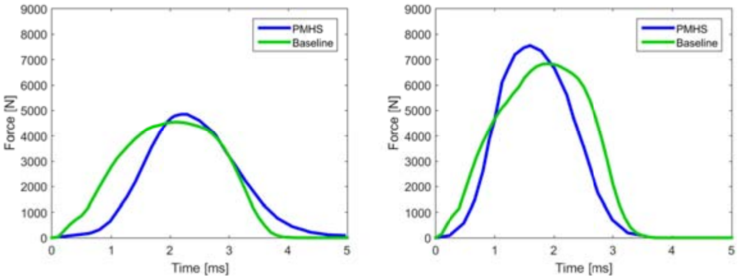

(a) drop height 15 cm (b) drop height 30 cm

Figure A 1. Comparison of head impact forces between the baseline model and PMHS response [19].

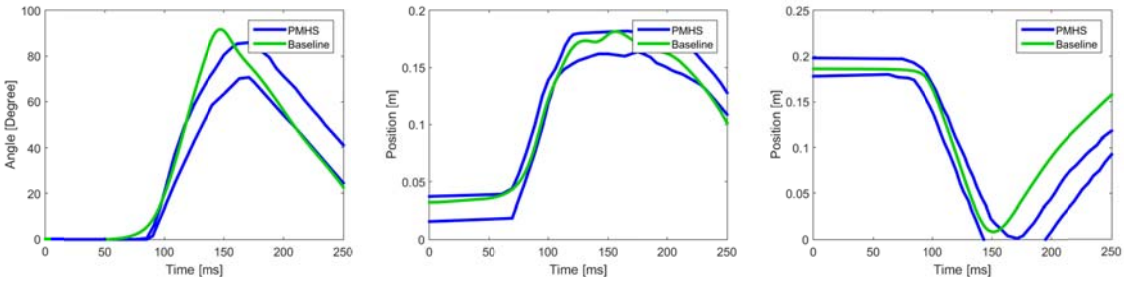

Figure A 2. Comparison of neck frontal flexion between the baseline model and corridor [29].

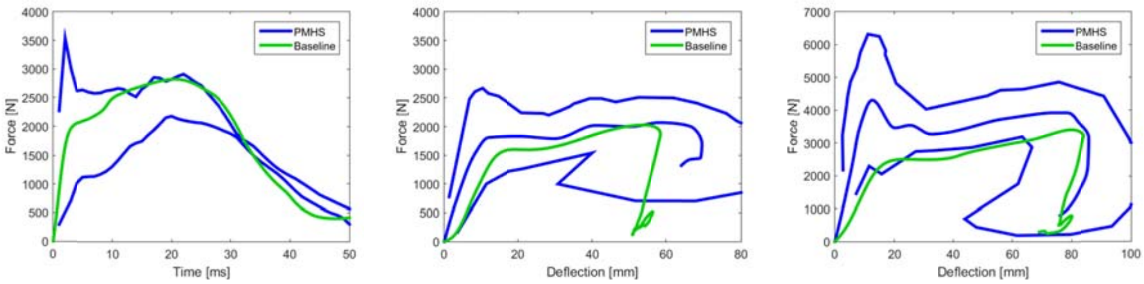

(a) thorax force 5.8m/s [22] (b) thorax stiffness 4.3 m/s [32] (c) thorax stiffness 6.7 m/s [32]

Figure A 3. Comparison of thorax forces and stiffens between the baseline model and corridor.

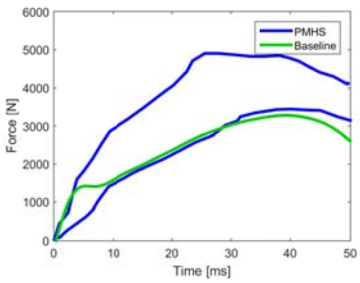

Figure A 4. Comparison of abdomen forces between the baseline model and corridor 6.1m/s [12].

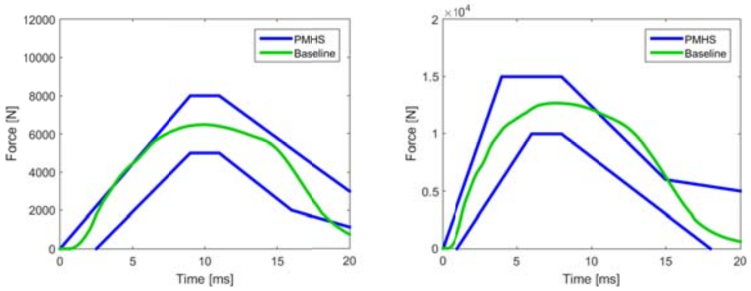

(a) pelvis force 4.5m/s (b) pelvis force 9.66m/s

Figure A 5. Comparison of pelvis forces between the baseline model and corridor [21].

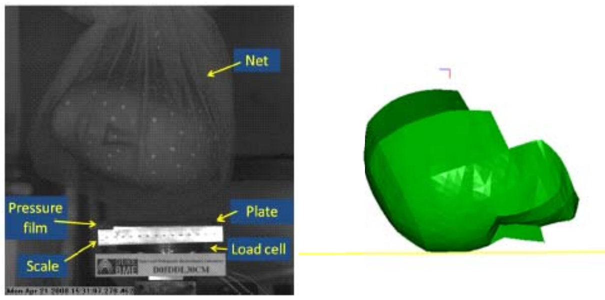

Figure B 1.Head drop set-up (forehead region) (Loyd et al., 2011).

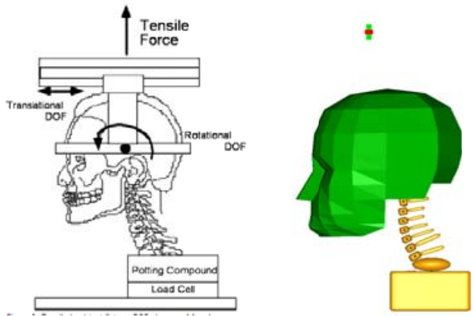

Figure B 2.Tensile head-neck load fixtures (Ouyang et al., 2005).

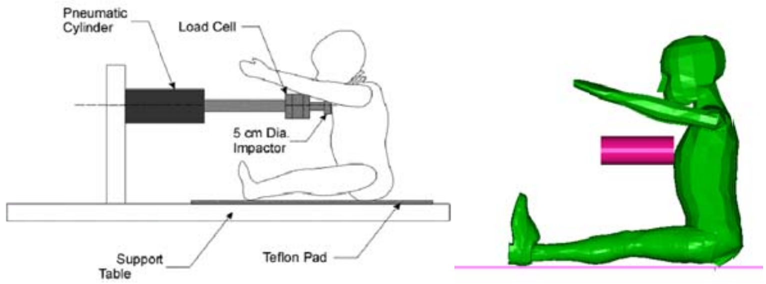

Figure B 3. Ouyang frontal thoracic impact test and simulation set-ups.

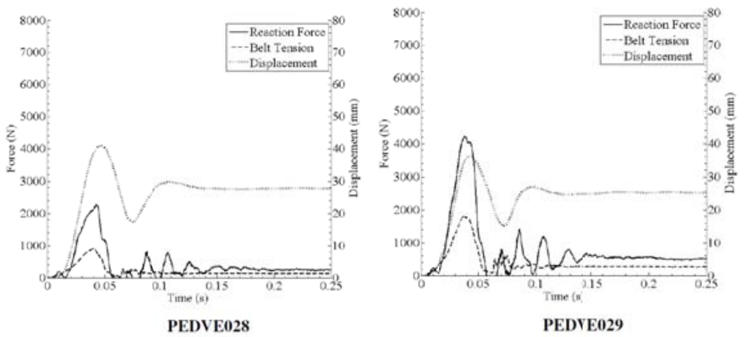

(a) (5 mm-wide belt) (b) 6YO (168 mm-wide belt);

Figure B 4. 6YO thorax input belt displacement functions [9].

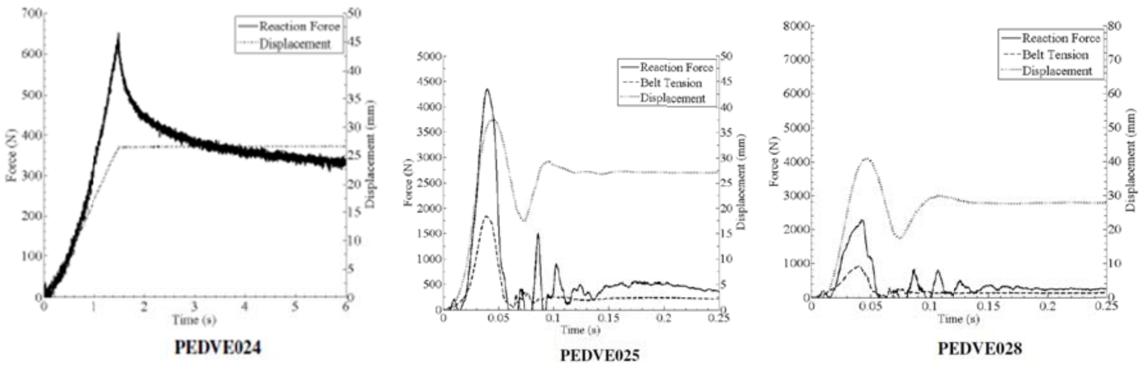

(a) lower abdomen, quasi-static (b) lower abdomen, dynamic (c) upper abdomen, dynamic

Figure B5. 6YO abdomen input belt displacement functions [9].

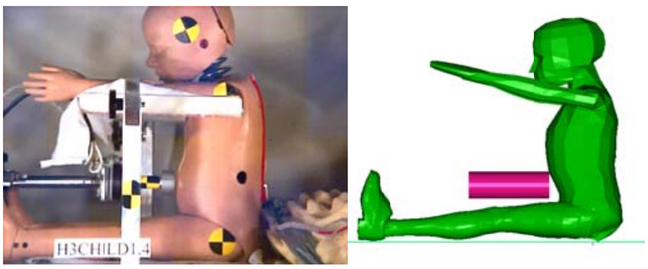

Figure B 6. Ouyang frontal abdominal impact test and simulation setups.

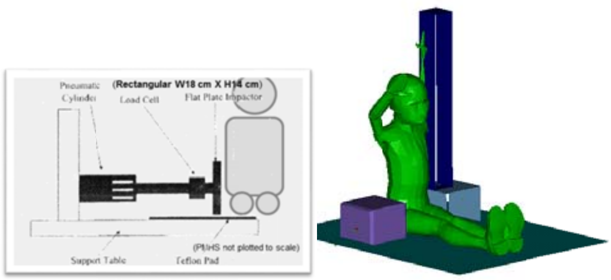

Figure B 7. Ouyang pelvis lateral impact test and simulation setups.